




Magnetron sputtering technique for analyzing the influence of RF sputtering power on microstructural surface morphology of aluminum thin films deposited on SiO₂/Si substrates

Somayeh Asgary¹ · Elnaz Vaghri² · Masoumeh Daemi³ · Parisa Esmaili⁴ · Amir H. Ramezani¹ · Saim Memon⁵ · Siamak Hoseinzadeh⁶ 

Received: 8 July 2021 / Accepted: 29 August 2021
© The Author(s) 2021

Abstract

In this research, aluminum (Al) thin films were deposited on SiO₂/Si substrates using RF magnetron sputtering technique for analyzing the influence of RF sputtering power on microstructural surface morphologies. Different sputtering RF powers (100–400 W) were employed to form Al thin films. The characteristics of deposited Al thin films are investigated using X-ray diffraction pattern (XRD), scanning electron microscopy (SEM), atomic force microscopy (AFM) and Fourier-transforms infrared (FTIR) spectroscopy. The X-ray diffraction (XRD) results demonstrate that the deposited films in low sputtering power have amorphous nature. By increasing the sputtering power, crystallization is observed. AFM analysis results show that the RF power of 300 W is the optimum sputtering power to grow the smoothest Al thin films. FTIR results show that the varying RF power affect the chemical structure of the deposited films. The SEM results show that by increasing the sputtering power leads to the formation of isolated texture on the surface of substrate. In conclusion, RF power has a significant impact on the properties of deposited films, particularly crystallization and shape.

Keywords Aluminum thin films · Grain size · Magnetron sputtering · RF power · FTIR

1 Introduction

Aluminum (Al) thin films are widely used in optical and microelectronic applications. These thin films have attracted a considerable attention in both academic and industrial

communities due to their remarkable properties and characteristics such as high reflectance, low resistivity, high conductance, better adhesion, resistance to oxidation and corrosion [1, 2] and novel optical properties [3, 4]. A significant scope of the Al thin films and tungsten oxide thin films [5, 6], specifically in the formation of composite for industrial aircraft applications. Recently, the optimum dielectric performance of polymer nanocomposites and improvement of the mixed conductivities have been explored by [7, 8]. Due to these outstanding properties, Al thin films find wide applications can also be in microelectronics systems, semi-conductors and optics components [2]. Furthermore, the interest in Al thin films has been exponentially increased due to depositions have been achieved utilizing a broad spectrum of substrates including mild steels, titanium, stainless steel, silver, silicon (100), polyethylene terephthalate (PET), polycarbonates and glass [2, 9]. Al films deposited on substrates are the most commonly utilizes surface coatings for aspheric mirrors, because Al is a good light reflector in the visible region and an extraordinary reflector in the mid and far infrared (IR) regions [10, 11]. In addition, other applications of Al thin films in different industrial fields include thin

✉ Siamak Hoseinzadeh
siamak.hosseinzadeh@uniroma1.it

¹ Department of Physics, West Tehran Branch, Islamic Azad University, Tehran, Iran

² Young Researchers and Elite Club, Shahr-E-Qods Branch, Islamic Azad University, Tehran, Iran

³ Department of Physics, Urmia branch, Islamic Azad University, Urmia, Iran

⁴ Young Researchers and Elite Club, Urmia branch, Islamic Azad University, Urmia, Iran

⁵ Solar Thermal Vacuum Engineering Research Group, School of Engineering, London Centre for Energy Engineering, London South Bank University, London SE1 0AA, UK

⁶ Department of Planning, Design, Technology, Sapienza University of Rome, Via Flaminia 72, 00196 Rome, Italy

film transistors [12], near-field fiber-optic probes [13], solar cells [14] and flat-panel displays [15].

Al thin films can be synthesized by various methods such as evaporation and sputtering, which can employ either thermal or electron beam sources [16, 17]. In general, sputter deposition is more suitable for materials with higher melting points, which are difficult to evaporate.

Among these methods, sputtering has attracted a great deal of interest due to its many concurrent advantages like; low substrate temperature, ability to produce reasonable quality thin films at a high deposition rate, good surface roughness and low cost [18, 19]. This technique has several advantages, including excellent control of film thickness, the fabrication of high-density film and high-quality aluminum oxide films. This technique allows precise control of purity, composition and stoichiometry of the films.

It is well known that the deposition conditions such as substrate temperature, deposition rates, sputtering power, substrate type and bias voltage have effects on the properties of thin films [2, 20]. In the past few years, many experimental studies were focused on the effects of sputtering RF power on the characteristics of the deposited films. For example; Dhar et al. have analyzed the effect of sputtering power, operating pressure and deposition temperature on the properties of Mo thin films grown on Mo sheet and soda–lime glass (SLG) [21]. Mahdhi et al. have investigated the influence of sputtering power on the properties of thin layers of GZO for photovoltaic applications [22]. Murugan et al. have performed studies about the effect of RF power on the properties of magnetron sputtered CeO₂ thin films [23, 24]. Zhao et al. have studied on effects of power on properties of ZnO thin films grown by radio frequency magnetron sputtering [25].

Even though extensive research has been carried out on the effects of RF power on the characteristics of various deposited films, there are very scarce works focused on the effect of sputtering power on the characteristic of the sputtered Al thin films. The novelty of this research is the experimental investigation the microstructure characteristics, roughness and optical properties of Al thin films deposited by RF sputtering at varying powers of 100 W, 200 W, 300 W and 400 W at a substrate temperature of 150 °C.

2 Experimental methodology

Al thin films were deposited using RF magnetron sputtering setup on SiO₂/Si substrates with an Al target (purity of 99.9999%). All the substrates were cleaned ultrasonically in acetone, isopropanol and deionized (DI) water for 15 min, respectively, to remove any residual contaminants prior to deposition.

The samples introduced into the RF sputtering chamber and then it was pumped to high vacuum pressure of 8.6 Torr $\times 10^{-6}$ (1.14 Pa $\times 10^{-3}$) achieved with rotary pump and turbomolecular pump. Argon gas (inert gas) was purged into the chamber with a flow of 3 sccm for sputtering process. The distance between the target and the substrate in our experimental condition was ≈ 7 cm. The Al target was pre-sputtered for 10 min to decontaminate and remove impurities before performing the depositions. Al thin films were deposited on the SiO₂/Si substrates at different sputtering powers from 100 to 400 W by maintaining other deposition conditions. The details of the sputtering conditions during the deposited of Al films are given in Table 1.

The generated samples were characterized using a range of analytical methods. The crystal structures of the deposited films were analyzed using a Cu-K α radiation ($k = 1.54060 \text{ \AA}$) of STOE SIADI MP diffractometer. The surface morphology of the samples was investigated by Hitachi, S-3400 emission scanning electron microscopy (SEM). Fourier-transforms infrared (FTIR) spectroscopy with a PerkinElmer spectrometer at a resolution of 8 cm⁻¹ in the range of 500–3800 cm⁻¹ was employed to investigate the bonding structures of the deposited samples. The topography of the surface and roughness of the deposited films were investigated by atomic force microscopy (AFM) (Dual Scope TM DS) analysis.

3 Result and discussion

3.1 X-Ray diffraction analysis (XRD)

The X-ray diffraction patterns of the films deposited on SiO₂/Si substrates, at different RF powers are shown in Fig. 1. In Fig. 1(a) and (b) labels show low sputtering powers of 100 W and 200 W, respectively, there was no peak in their XRD pattern and the deposited films indicate non-crystalline feature. As the sputtering power increases to 300 leading to 400 W, new diffraction peaks at $2\theta = 30.9^\circ$ and $2\theta = 61.6^\circ$ corresponding to (001) and (430) reflection planes of orthorhombic aluminum silicene oxide structure (JCPDS card No. 002–0428 and 002–0469) observed in the

Table 1 List of the deposition parameters utilized to deposit the Al thin films on SiO₂/Si substrate

Process parameters	Value
Target to substrate distance (cm)	7
RF power (W)	100–400
Substrate temperature (°C)	150
Base pressure (Torr)	8.6×10^{-6}
Deposition time	15(minute)
Working pressure (Torr)	9×10^{-4}

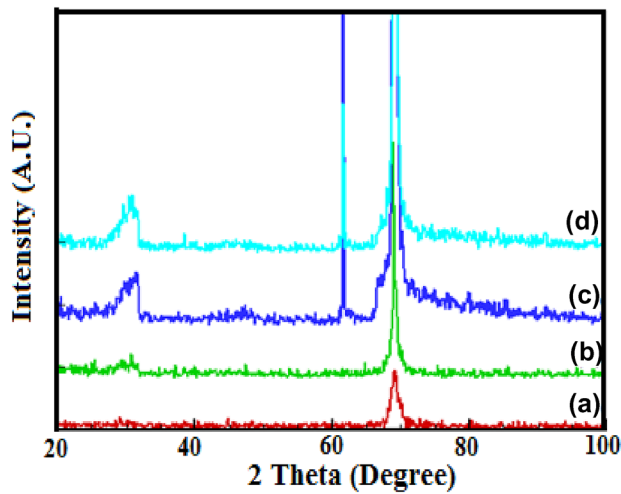


Fig. 1 X-ray diffraction pattern of the Al thin films deposited on SiO₂/Si substrate at different RF powers of shown in label (a) 100 W, (b) 200 W, (c) 300 W and (d) 400

XRD pattern of the deposited films, as shown in Fig. 1, label (a) and (b). Furthermore, in Fig. 1 label (c) shows the peak at $2\theta = 80.01^\circ$ also attributed to X-ray photons diffracted from aluminum silicone oxide structure (JCPDS card No. 002–0413). The appearance of these diffraction peaks at higher sputtering powers may be attributed to surface diffusion of Al sputtered atoms on the substrate. It seems that

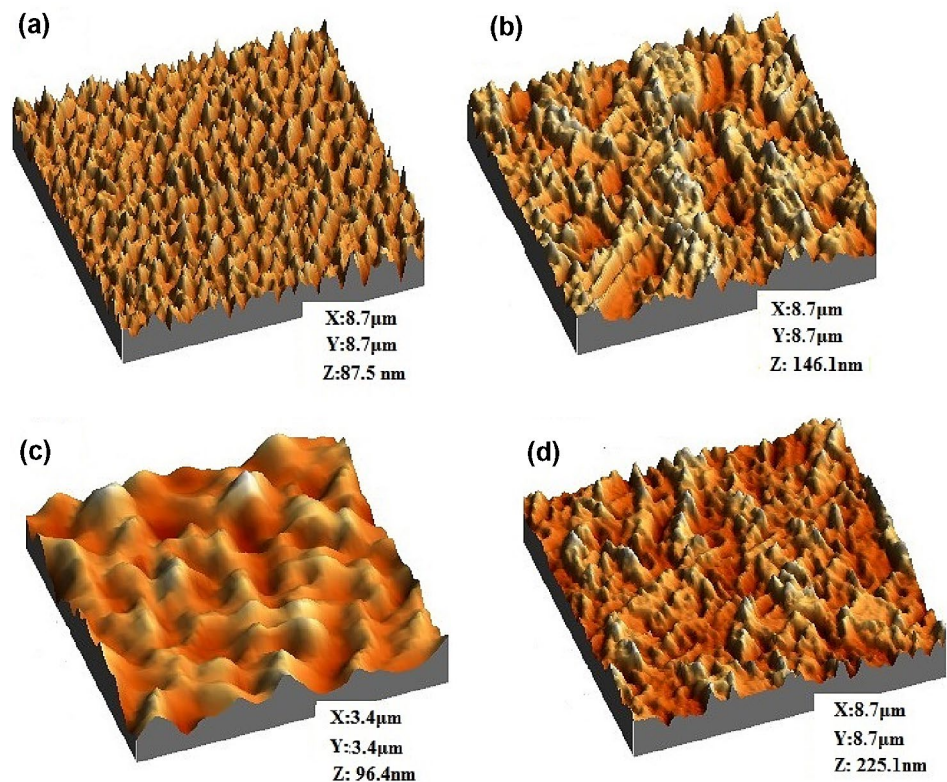
higher RF power enhanced mobility energy of Al sputtered atoms on the surface of the substrate to diffuse in the substrate during growth stage and formed a new phase of aluminum silicone oxide. In other word, higher sputtering power induced high incident ion energy, resulting in high surface mobility and mean diffusion path of sputtered atoms [26]. In addition, X-ray diffraction pattern, Fig. 1 label (d) exhibits a weak diffraction peak around 38.3° belongs to the (111) reflection planes of aluminum structure (JCPDS card No. 004–0787). Moreover, a peak of X-ray photons diffracted (111) planes of Si substrate lattice structure can be seen a $2\theta = 69.6^\circ$. Increasing the intensity of diffraction peaks by increasing the RF power confirms a better crystallinity of the samples at higher RF powers. By increasing the sputtering power, the sputtering yield becomes high and the sputtered particles are ejected with higher energy and the growth of a more crystallized phase [26]. It seems that the peak at $2\theta = 61.6^\circ$ is the preferred crystalline orientation in higher RF power and is so strong in 300 W.

3.2 Surface morphological analysis

3.2.1 Surface roughness

The surface roughness was analyzed using atomic force microscopy (AFM) in contact mode for all samples. Figure 2 illustrates the three-dimensional-AFM micrographs of the Al

Fig. 2 3D AFM images of Al films deposited on SiO₂/Si substrate at various sputtering powers: **a** 100 W, **b** 200 W, **c** 300 W and **d** 400 W



films deposited at different sputtering powers. The root mean squared (RMS) roughness of surface is the main parameters for the characterization of the surface structure [27, 28].

$$\text{RMS} = \sqrt{\frac{\sum_{n=1}^N (Z_n - \bar{Z})^2}{N - 1}}$$

where \bar{Z} is the average height and N is the number of data points. The roughness of the films deposited at different RF powers is plotted in Fig. 3. The RMS roughness of the as-deposited film initially rose to 16.95 nm when the sputtering power was raised to 200 W, as shown in Fig. 3. Thereafter, it decreased to 12.16 nm when the deposition increased to 300 W. This behavior may be explained in the following way: (i) At a low RF power of 200 W, the atoms or ions have low energy and tended to 'stay' at the site of its arrival, thus creating a much rougher surface [26, 29]; (ii) At a high RF power of 300 W, the kinetic energy of the incoming atoms, particles or ions, increases that enhances the lateral diffusion of the ions or particles, and then the surface roughness decreases. Moreover, it was discovered that as the RF power was increased to 400 W, the roughness increased. This may be attributed to the fact that the higher power improved the energy of the incoming ionized species and decreased the rearrangement time of the atoms on the substrate before arrival of next atoms [29, 30], which thereby resulted in higher surface roughness [26].

At high RF power, the argon gas and the deposition particles inside the sputtering chamber acquire very kinetic high energy, which may lead to: (i) high deposition rate, growth and recrystallization leading to large grain sizes, (ii) excess collisions between target atoms and ions reducing

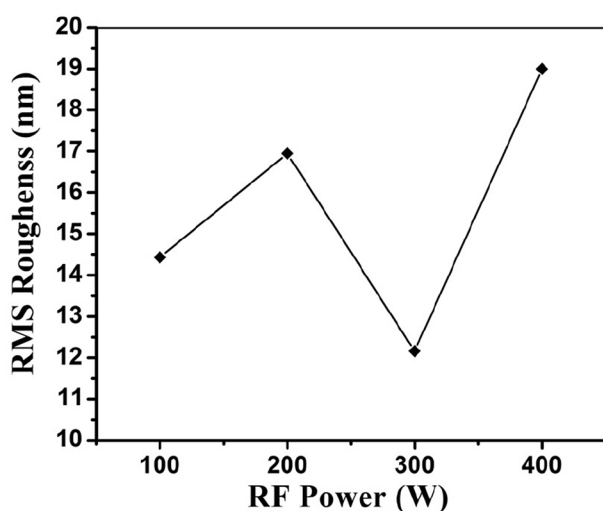


Fig. 3 The RMS roughness of Al thin films deposited on SiO₂/Si substrate as a function of sputtered RF power

the mean-free-path of the target atoms and therefore lowering sputtering yield and hence less crystallization and film growth [31, 32]. The results presented in sample 2 and 4 can well be attributed to the first reason.

Although the RMS values are highly influenced by the RF power, our result shows that there exists no direct correlation between the increase in RF power and RMS values. The finest and well-defined grained microstructure was observed at the power of 300 W and the highest RMS roughness values are obtained on the surface of films sputtered at a power of 400 W. According to our study, the RF power of 300 W is the optimum condition for deposition of Al thin film.

3.2.2 Scanning electron microscopy analysis (SEM)

Figure 4 illustrates the SEM micrographs of the deposited films showing, at lower RF powers, the deposited films are composed of small, homogenous and well-defined grains. In addition, interconnected porous structures between the grains were observed. The presence of these porous structures is attributed to the high roughness values. The SEM images indicate that with an increase of RF power led to the growth of larger grains. In fact, with increasing sputtering RF power, the deposition particles did not have enough time to latterly diffuse on the substrate, and accumulated together to form larger grains [26]. This result is in good agreement with the results of AFM analysis.

3.2.3 FT-IR characterization

The Fourier-transformed infrared spectroscopy (FT-IR) is an analytical technique which is used to investigate the chemical structure and molecular bonding of the materials. The infrared spectra of the produced samples in the range of 500–3800 cm⁻¹ are depicted in Fig. 5. In the lower frequency region, the minor absorption peak (low intensity) appearing at around 619 cm⁻¹ can be assigned to a coupled Al-O and Si-O (out-of-plane) bond [33, 34]. Furthermore, the absorption peak which is located at around 655 cm⁻¹ is arising from in-plane Al-O vibration rather than Al-O-Si vibration [35]. According to the literatures [34, 36], the presence of weak absorption peaks at about 669 cm⁻¹ and 684 cm⁻¹ is related to the vibrations modes of Si-O band. Moreover, the absorption band at 694 cm⁻¹ is corresponding to symmetrical bending vibrations of Si-O whereas vibration band at 792 cm⁻¹ can be attributed to symmetrical stretching vibrations of Si-O [37]. Furthermore, the characteristic vibration at 937 cm⁻¹ can be assigned to O-Si-O bond [38]. Besides, the absorption band at about 943 cm⁻¹ can be associated with stretching mode of Si-OH [39]. The infrared absorption band at 1118 cm⁻¹ is attributed to the tetrahedral stretching vibration of silicon-apical oxygen (Si-O) [40]. Moreover, the absorption bands

Fig. 4 SEM images of the Al thin films deposited on SiO₂/Si substrate at different RF Powers: **a** 100 W, **b** 200 W, **c** 300 W and **d** 400 W

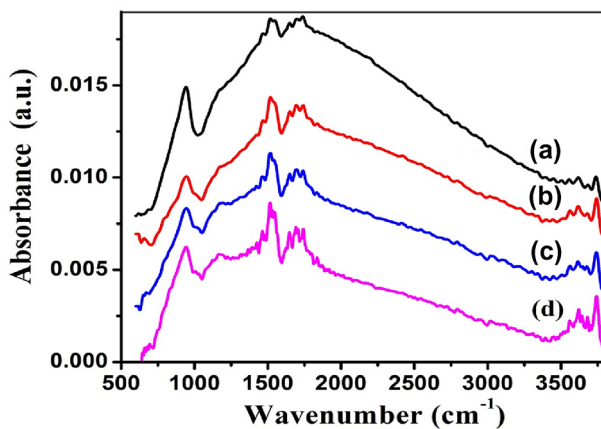
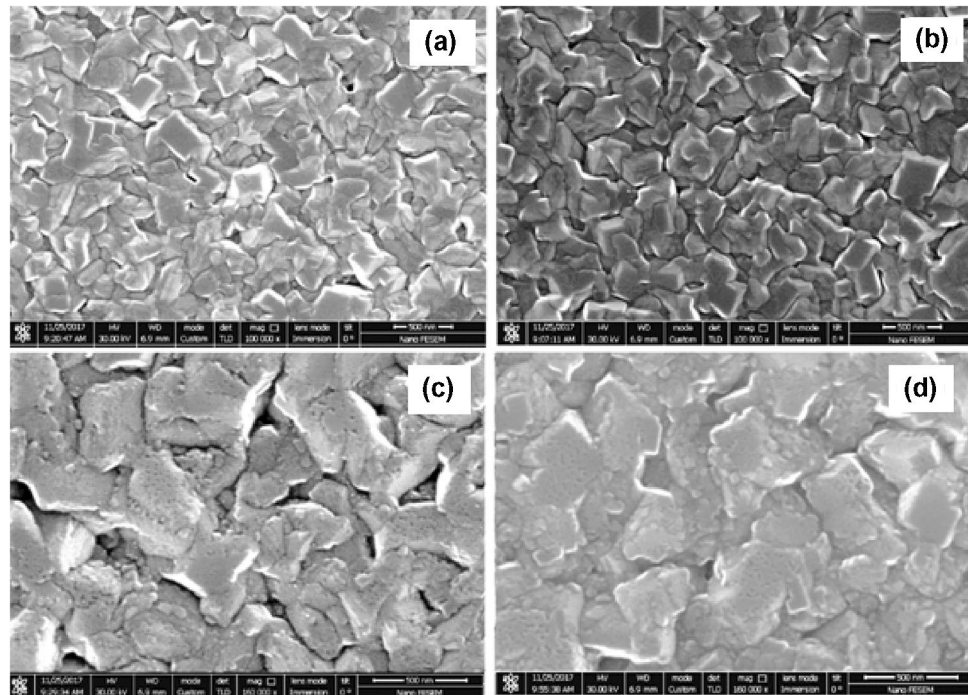


Fig. 5 FTIR spectra of the Al thin films deposited on SiO₂/Si substrate at different RF powers: **(a)** 100 W, **(b)** 200 W, **(c)** 300 W and **(d)** 400 W

at about 1164 cm⁻¹ and 1649 cm⁻¹ can be related to the antisymmetric stretching vibrations mode of Si-O-Si of silica and O-H deformation, respectively [41]. Furthermore, the bands in the range of 1300–1516 cm⁻¹ are assigned to the Si-O-Si stretching bands of low “crystallinity” phases, mainly amorphous silica [38]. In addition, in the higher frequency region, the absorption bands at approximately 3554 cm⁻¹, 3616 cm⁻¹ and 3741 cm⁻¹ are attributed to the OH stretching modes of Al (OH) Si [42] and (Al Al) O-OH [43] Si-OH groups, respectively. The observation of OH stretching modes in all the samples may be due to

the presence of silicate in the substrate. Furthermore, the FTIR results show that the varying RF power affect the chemical structure of the deposited films [44].

The intensity of an absorption band in FTIR spectra depends on the number of the specific bonds present [45].

4 Conclusions

In this study, Al thin films were deposited on the SiO₂/Si substrates by RF magnetron sputtering system, and the influence of the RF power on the structure and surface morphology of the deposited films was investigated experimentally. The study of structural properties implicate that the sample deposited at 300 W has lower RMS roughness and smooth surface, this is because the kinetic energy of the incoming atoms, particles or ions, increases and led to enhances the lateral diffusion of the ions or particles. The results reveal that when the sputtering power was increased to 400 W, the deposition particles did not have enough time to disperse over the substrate and clumped together to form larger grains, increasing surface roughness. It is concluded that increasing the sputtering power enhanced the crystallinity of the deposited films, while altering the sputtering power affected the chemical structure of the deposited films. This paper findings show that the RF power influences the characteristics of deposited films, and that by changing the sputtering power, the desired morphological structure and properties may be tuned.

Funding Open access funding provided by Università degli Studi di Roma La Sapienza within the CRUI-CARE Agreement.

Open Access This article is licensed under a Creative Commons Attribution 4.0 International License, which permits use, sharing, adaptation, distribution and reproduction in any medium or format, as long as you give appropriate credit to the original author(s) and the source, provide a link to the Creative Commons licence, and indicate if changes were made. The images or other third party material in this article are included in the article's Creative Commons licence, unless indicated otherwise in a credit line to the material. If material is not included in the article's Creative Commons licence and your intended use is not permitted by statutory regulation or exceeds the permitted use, you will need to obtain permission directly from the copyright holder. To view a copy of this licence, visit <http://creativecommons.org/licenses/by/4.0/>.

References

1. K. Bordo, H. Rubahn, Effect of deposition rate on structure and surface morphology of thin evaporated Al films on dielectrics and semiconductors. *Mater. Sci.* **18**, 13 (2012). <https://doi.org/10.5755/j01.ms.18.4.3088>
2. F.M. Mwema, O.P. Oladijo, S.A. Akinlabi, E.T. Akinlabi, Properties of physically deposited thin aluminium film coatings: a review. *Alloy. Compd.* **747**, 306 (2018). <https://doi.org/10.1016/j.jallcom.2018.03.006>
3. S.B. Mansoor, B.S. Yilbas, Phonon transport in a curved aluminum thin film due to laser short pulse irradiation. *Opt. Laser Technol.* **101**, 107 (2018)
4. G. Beck, S. Funk, Correlation between optical appearance and orientation of aluminum. *Surf. Coat. Technol.* **206**, 2371 (2012)
5. G. Tan, D. Tang, D. Dastan, A. Jafari, Z. Shi, Q. Chu, J. Silva, X. Yin, Structures, morphological control, and antibacterial performance of tungsten oxide thin films. *Ceram. Int.* **47**, 17153–17160 (2021)
6. G. Tan, D. Tang, D. Dastan, A. Jafari, J. Silva, X. Yin, *Mater. Sci. Semicond. Process* **122**, 105506 (2021)
7. W. Zhang, X. Zhu, L. Liang, P. Yin, P. Xie, D. Dastan, K. Sun, R. Fan, Z. Shi, Significantly enhanced dielectric permittivity and low loss in epoxy composites incorporating 3d W-WO₃/BaTiO₃ foams. *J Mater Sci* **56**, 4254–4265 (2021)
8. Y. Jiao, Z. Huang, W. Hu, X. Li, Q. Yu, Y. Wang, Y. Zhou, D. Dastan, In-situ hybrid Cr₃C₂ and γ' -Ni₃(Al, Cr) strengthened Ni matrix composites: microstructure and enhanced properties. *Mater. Sci. Eng. A* **820**(2021), 141524 (2021)
9. K. Shan, Z. Yi, X. Yin, D. Dastan, S. Dadkhah, B. Coates, H. Garmestani, Mixed conductivities of A-site deficient Y, Cr-doubly doped SrTiO₃ as novel dense diffusion barrier and temperature-independent limiting current oxygen sensors. *Adv. Powder Technol.* **31**, 4657–4664 (2020)
10. E.A. Esfahani, H. Salimijazi, M.A. Golozar, J. Mostaghimi, L. Pershin, A comprehensive review of corrosion resistance of thermally-sprayed and thermally-diffused protective coatings on steel structures. *Therm. Spray. Techn.* **21**, 1195 (2012). <https://doi.org/10.1007/s11666-019-00855-3>
11. M.G. Faraj, K. Ibrahim, Investigation of the structural properties of thermally evaporated aluminium thin films on different polymer substrates. *Int. J. Thin. Film. Sci. Tech.* **4**, 17 (2015). <https://doi.org/10.12785/ijtfsv040106>
12. C. Jaing, *J. Opt. Quant. Electron* **28**, 1583 (1996)
13. H. Takatsuji, T. Arai, Pinholes in Al thin films: their effects on TFT characteristics and a taguchi method analysis of their origins. *Vacuum* **59**, 606 (2000). [https://doi.org/10.1016/S0042-207X\(00\)00323-7](https://doi.org/10.1016/S0042-207X(00)00323-7)
14. C.W. Hollars, R.C. Dunn, Evaluation of thermal evaporation conditions used in coating aluminum on near-field fiber-optic probes. *Rev. Sci. Instrum.* **69**, 1747 (1998). <https://doi.org/10.1063/1.1148836>
15. H. Shinohara, H. Morooka, I. Ikeo, A. Takenouchi, S. Nakajima, Y. Arai, Solar Cell and Method for Producing Electrode for Solar Cell, United States Patent US005891264A, 1999.
16. A.T. Voutsas, Y. Hibino, R. Pethe, E. Demaray, Structure engineering for hillock-free pure aluminum sputter deposition for gate and source line fabrication in active-matrix liquid crystal displays. *Vac. Sci. Technol. A* **16**, 2668 (1998). <https://doi.org/10.1116/1.581398>
17. G. Kaune, E. Metwalli, R. Meier, V. Körstgens, K. Schlage, S. Couet, R. Röhlberger, S.V. Roth, P. Müller-Buschbaum, Growth and Morphology of Sputtered Aluminum Thin Films on P3HT Surfaces. *ACS Appl. Mater. Interfaces* **3**, 1055 (2011)
18. X. Yu-Qing, L. Xing-Cun, C. Qiang, L. Wen-Wen, Z. Qiao, S. Li-Jun, L. Zhong-Wei, W. Zheng-Duo, Y. Li-Zhen, Characteristics and properties of metal aluminum thin films prepared by electron cyclotron resonance plasma-assisted atomic layer deposition technology. *Chin. Phys. B* **21**, 078105 (2012)
19. M.J. Lee, T.I. Lee, J. Lim, J. Bang, W. Lee, T. Lee, J.M. Myoung, Effect of the deposition temperature and a hydrogen post-annealing treatment on the structural, electrical, and optical properties of Ga-doped ZnO films. *Electron. Mater. Lett.* **5**, 127 (2009). <https://doi.org/10.3365/eml.2009.09.127>
20. H.W. Wu, R.Y. Yang, Ch.M. Hsiung, Ch.H. Chu, Influence of sintering temperatures of ceramic targets on microstructures and photoelectric properties of titanium-doped ZnO nano-films. *Mater. Sci.: Mater. Electron.* **24**, 166 (2013). <https://doi.org/10.1007/s10854-016-6104-y>
21. H. Khachatryan, S.N. Lee, K.B. Kim, H.K. Kim, M.J. Kim, Al thin film: the effect of substrate type on Al film formation and morphology. *Phys. Chem. Solids* **122**, 109 (2018). <https://doi.org/10.1016/j.jpccs.2018.06.018>
22. N. Dhar, P. Chelvanathan, M. Zaman, K. Sopian, N. Amin, An investigation on structural and electrical properties of rf-sputtered molybdenum thin film deposited on different substrates. *Energy Procedia* **33**, 186 (2013). <https://doi.org/10.1016/j.egypro.2013.05.057>
23. H. Mahdhi, Z.B. Ayadi, J.L. Gauffier, K. Djessas, S. Alaya, Influence of sputtering power on the properties of thin layers of GZO for photovoltaic applications. *J. Mater. Sci. Mater. El.* **26**, 3336 (2015). <https://doi.org/10.1007/s10854-015-2836-3>
24. R. Murugan, G. Vijayaprasath, T. Mahalingam, Y. Hayakawa, G. Ravi, Effect of rf power on the properties of magnetron sputtered CeO₂ thin films. *J. Mater. Sci. Mater. El.* **26**, 2800 (2015). <https://doi.org/10.1007/s10854-015-2761-5>
25. Y.J. Zhao, D.Y. Jiang, M. Zhao, R. Deng, J.M. Qin, S. Gao, Q.C. Liang, J.X. Zhao, Effects of power on properties of ZnO thin films grown by radio frequency magnetron sputtering. *Appl. Surf. Sci.* **266**, 440 (2013). <https://doi.org/10.1016/j.apsusc.2012.12.055>
26. Zh. Chen, W. Tian, X. Zhang, Y. Wang, Effect of deposition parameters on surface roughness and consequent electromagnetic performance of capacitive RF MEMS switches: a review. *Micro-mechanics Microengineering* **27**, 113003 (2017). <https://doi.org/10.1088/1361-6439/aa8917>
27. A. Mallikarjuna Reddy, A. Sivasankar Reddy, K.S. Lee, P. Sreedhara Reddy, Growth and characterization of NiO thin films prepared by dc reactive magnetron sputtering. *Solid State Sc.* **13**, 314(2011). <https://doi.org/10.1016/j.solidstatesciences.2010.11.019>

28. E. Vaghri, Z. Khalaj, M. Ghoranneviss, M. Borghei, Characterization of diamond-like carbon films synthesized by DC-plasma enhanced chemical vapor deposition. *Fusion Energy* **30**, 447 (2011). <https://doi.org/10.1007/s10894-011-9406-3>
29. J. Eskusson, R. Jaaniso, E. Lust, Synthesis of DLC films by PLD from liquid target and dependence of film properties on the synthesis conditions. *Appl. Phys. A*. **93**, 745 (2008). <https://doi.org/10.1007/s00339-008-4706-9>
30. V. Bhatt, S. Chandra, Silicon dioxide films by RF sputtering for microelectronic and MEMS applications. *J. Micromech. Microeng* **17**, 1066 (2007). <https://doi.org/10.1088/0960-1317/17/5/029>
31. A. Kale, R.S. Brusa, A. Miotello, Structural and electrical properties of AlN films deposited using reactive RF magnetron sputtering for solar concentrator application. *Appl. Surf. Sci.* **258**, 3450 (2012). <https://doi.org/10.1016/j.apsusc.2011.11.095>
32. K. Wasa, S. Hayakawa, *Handbook of Sputter Deposition Technology* (Noyes Publications, New Jersey, 1992)
33. F.M. Mwema, O.P. Oladijo, E.T. Akinlabi, *Mater. Today Proc.* **5**(9/3), 20464 (2018)
34. A. Gupta, V. Amitabh, B. Kumari, B. Mishra, FTIR and XRPD studies for the mineralogical composition of jharkhand bentonit. *Res. J. Pharm. Biol. Chem. Sci.* **4**, 361 (2013)
35. J. Madejova, P. Komadel, Baseline studies of the clay minerals society source clays: infrared methods. *Clays Clay Mineral* **49**, 410 (2001). <https://doi.org/10.1346/CCMN.2001.0490508>
36. D.M. Jenkins, Empirical study of the infrared lattice vibrations (1100–350 cm⁻¹) of phlogopite. *Phys. Chem. Mineral* **16**, 408 (1989). <https://doi.org/10.1007/BF00199563>
37. A. Paula dos Santos Pereira, M. Henrique Prado da Silva, E. Pereira Lima Júnior, A. dos Santos Paula, F. James Tommasini, Processing and Characterization of PET Composites Reinforced With Geopolymer Concrete Waste. *Mater. Res.* **20**, 411 (2017). <https://doi.org/10.1590/1980-5373-mr-2017-0734>.
38. T. Ahmad, K. Ahmad, M. Alam, Characterization and constructive utilization of sludge produced in clari-flocculation unit of water treatment plant. *Mater. Res. Express* **5**, 035511 (2018). <https://doi.org/10.1088/2053-1591/aab23a>
39. T. Hurma, Optical Vibrational And Morphological Properties Of S-Co3o4 Nanostructured Thin Film. *Sci. and Technology A, Appl. Sci. and Eng.* **18**, 388 (2017). <https://doi.org/10.18038/aubtda.295720>.
40. M. Catauro, F. Papale, F. Bollino, S. Piccolella, S. Marciano, P. Nocera, S. Pacifico, Silica/quercetin sol-gel hybrids as antioxidant dental implant materials. *Sci. Technol. Adv. Mater.* **16**, 035001 (2015). <https://doi.org/10.1088/1468-6996/16/3/035001>
41. K. Kitajima, N. Takusagawa, Effects of tetrahedral isomorphous substitution on the IR spectra of synthetic fluorine micas. *Clay Miner.* **25**, 235 (1990). <https://doi.org/10.1180/claymin.1990.025.2.08>
42. M. Diko, G. Ekosse, J. Ogola, Fourier transform infrared spectroscopy and thermal analyses of kaolinitic clays from south africa and cameroon. *Acta Geodyn. Geomater* **13**, 149 (2016). <https://doi.org/10.13168/AGG.2015.0052>
43. J. Antonio Cecilia, L. Pardo, M. Pozo, E. Bellido, F. Franco. Microwave-Assisted Acid Activation of Clays Composed of 2:1 Clay Minerals: A Comparative Study. *Minerals* **8**, 376 (2018). <https://doi.org/10.3390/min8090376>.
44. N. Tabatabaai, D. Dorrani, Effect of fluence on carbon nanostructures produced by laser ablation in liquid nitrogen. *Appl. Phys. A* **122**, 558 (2016)
45. M. Yang, M. Ye, H. Han, G. Ren, L. Han, Zh. Zhang, Spectroscopy (2018). <https://doi.org/10.1155/2018/6958260>

Publisher's Note Springer Nature remains neutral with regard to jurisdictional claims in published maps and institutional affiliations.